Title: Monitoring agricultural water budget under semi-arid conditions in southern Iran using Sentinel-2 to Landsat-8 datasets.

Arnaud Caiserman[a*], Farshad Amiraslani[b], Dominique Dumas[a]

Highlights:

- We assessed……………
- Retrieved water use by farmers from PyPySebal was accurate
- Crop areas classification with Sentinel-2 images through NDVI profiles was accurate
- PYSEBAL Land Surface Temperature influences ET variability more than Radiation
- The water balance of Marvdasht plain was negative

Abstract: This paper is a first attempt to compute the total water needs of an agricultural plain with remote sensing and ground data in Iran. First, the study mapped the cropping areas with Sentinels-2 images, based on NDVI profiles classification. Locations of 1253 crops were collected, from which NDVI profiles were extracted and used to classify the other unknown pixels. This model was validated and 85% of the areas were correctly classified. Second, the crop water needs were computed using PYSEBAL and Landsat-8 images. The crop evapotranspiration (ET_{season}) and net irrigation requirements (NIR_{season}) were calculated for every crop type. The key point was to validate PYSEBAL outputs, despite the lack of lysimeter data. We compared $NIR_{PYSEBAL}$ with 5 NIR from the ground data collected with farmers. $NIR_{PYSEBAL}$ underestimated the reality with an average of 10% while the overestimation average was 17%. The comparison of Daily ET from FAO-56 method and Daily ET PYSEBAL showed a RMSE of 0.67 mm/day and MAE of 0.52 mm/day, which assesses the accuracy of PYSEBAL. This dataset also showed wide ranges of NIR per crop type, depending on climate conditions, soil types and practices. ET_{season} varies according to weather parameters in the plain and NIR_{season}, according to different irrigation practices. In PYSEBAL, the most sensitive parameter for ET variability was Land Surface Temperature. This study targets the most sensitive crops by defining the pressure of its NIR on the available water, by diving NIR total with the volume of available precipitations for groundwater recharge. The most water demanding crops were identified: rice (NIR: 1427 mm) and corn (669). The total water balance of Marvdasht was negative in 2018 with 0.2859 km^3 of extracted groundwater for irrigation for only 0.098 km^3 of available water for aquifers recharge.

Key words: PyPySebal, Crop mapping, Iran, Agriculture, Irrigation, Water needs, Sentinel-2, Landast-8

1. Introduction

Countries are not equally affected by water shortage issues and they adopt different approaches for agricultural adaptation to droughts and climate change. Thereby, this study puts forward the case of Iran in the West of Asia as one of the countries severely affected by water issues (Faramarzi, 2010; Karimi et al., 2018; Keshavarz et al., 2014; Madani, 2014; Madani et al., 2016; Zehtabian et al., 2010). The country is facing a double challenge: (1) an increasing water needs due to growing population (Motamed, 2017; Neuve-Eglise, 2007; Saatsaz, 2019) and (2) an increase of drought frequency over the last two decades and future climate change scenarios (Golian et al., 2015; Keshavarz and Karami, 2013; Tabari et al., 2012; Amiraslani and Caiserman, 2018). However, Iran has attempted to increase the agricultural productivity with greater access to water for irrigation to support food security.

The objective of this paper is to identify sensitive crops which require significant amounts of irrigation in one of the most important agricultural zones of Iran (Hassanshahi et al., 2015; Moameni, 1999): the plain of Marvdasht in the Fars Province. For this purpose crop Evapotranspiration (ET_{Season}) and Net Irrigation Requirements (NIR_{season}) were computed using remote sensing. In addition, such an analysis of crop water needs enabled us to assess the total use of groundwater during that year. The Marvdasht Plain is fully in the prism of climate change as it records a decrease in rainfall of 1.1 mm/decades over the period 1988-2015 (Roshan and Negahban, 2015) as well as an increase in temperature of 0.05 to 0.99C°/decades since 1975 (Soltani et al., 2016). Droughts have also been frequent over the last forty years, particularly in 1981, 1982, 1983, 1985, 1987, 2003, 2004 2008 and 2011, during which drought severity strongly affected agricultural production (Ahani et al., 2012; Keshavarz et al., 2014; Keshavarz and Karami, 2013). These past and future climate changes make it essential to estimate water use by agriculture, as support to political decision-making for the decades to come. Monitoring water consumption of crops appears as a key issue to highlight the crops which might exacerbate water shortage, in the name of food security. Moreover, the assessment of water balance and NIR per crop type is the first attempt in this region. Remote sensing is a useful tool and has already proven its relevancy to monitor agriculture and water issues, especially under arid and semi-arid conditions (e.g. Caiserman et al., 2019).

The application of remote sensing in agriculture are subdivided as follows (Asgarian et al., 2016): (1) agricultural dynamics and the evolution of crop areas with low resolution images such as MODIS (250 m), (2) precision agriculture with high resolutions images such as Quickbird (0.65), Pleiade (0.7 m) or RapidEye images (5 m) for yields estimations, soil humidity assessment or weed prevention and (3) crop type classification with medium resolution images such as Landsat-8 (30 m) or Sentinel-2 (10 m). The present paper is considering the third approach of agriculture through crop mapping and crop water needs estimation. Numerous studies have already developed methodology to map crop areas with satelite images (Belgiu and Csillik, 2018; Hao et al., 2018; Heupel et al., 2018; Kenduiywo et al., 2018; Lamb and Brown, 2001; Panigrahy and Sharma, 1997; Song et al., 2017; Waldhoff et al., 2017; Xie et al., 2007; Zhong, 2012). This paper used a new process, recently developed for another case of study in Lebanon using Sentinel-2 images for its good resolution (10 m) (Caiserman et al., 2019). This method was divided in three steps: (a) a new way to extract fields boundaries by stacking monthly high NDVI pixels to highlight the cultivated areas, (b) the retrieval of crop calendars and (c) the classification of pixels. The novelty of this methodology was its simplicity and reproducibility. In addition, this crop mapping process was based on field works, increasing the reliability of the outputs. Remote sensing has another role for water needs estimations. Numerous algorithms have already been developed such as SEBI (Menenti and Choudhury, 1993), SEBS (Su, 2002), S-SEBI (Roerink et al., 2000), METRIC (Allen et al., 2007), TSM (Norman and Becker, 1995), SAMIR (Simonneaux et al., 2009) and PYSEBAL using Landsat-8 images (Bastiaanssen et al., 1998a, 1998b; Hessel, 2019; Hessel et al., 2017). This paper selected the latest version of PYSEBAL since it does not require a significant amount of data and its accuracy has been assessed in many countries between 85% and 95% on experimental fields (Liou and Kar, 2014). The validation was conducted with lysimeter measurements in several countries with Root Mean Square Error (RMSE) of 0.7 in Spain, 0,03 in China, 0.14 in Nigeria or 0,6 in Italy (Water Watch, 2019).

The second section of the paper introduces the chosen region in Iran and the requisite data from to ground to the satelite images to compute the agricultural water budget. In the third section, the results of crop mapping and PYSEBAL will be explained and interpreted. Eventually, the fourth section consists in the discussion of the paper, namely the validation of crop mapping and PYSEBAL through field works and global literature review, and the perspectives of these models will be shown in the same part.

2. Methods and materials

2.1 Study area: Marvdasht plain

The study area is located in the Fars Province, southern Iran (29°52'34N - 52°48′22E, elevation: 1600 m) and covers 95000 ha (figure 1). The current climate is the Mediterranean characterised by two contrasted seasons between wet winters and dry and hot summers. According to local climate stations, Marvdasht annually receives 440 mm in the northern part and 275 mm in the more arid area in the southern part and 73% of the precipitation occurs in winter (based on annual average on 1990-2017 period). Thereby, the irrigation is necessary from May until October and the annual average of potential evapotranspiration reaches 1680 mm (Attarod et al., 2016). Nevertheless, precipitations are highly variable and numerous droughts occurred in the recent decades (Ahani et al., 2012; Keshavarz et al., 2014; Keshavarz and Karami, 2013; Khosravi et al., 2017).

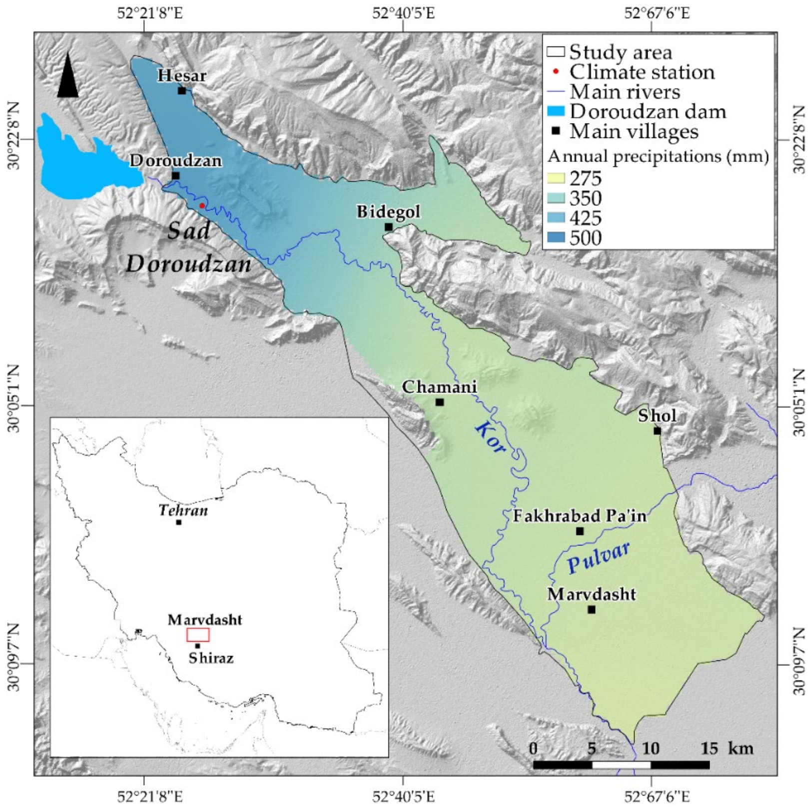

Figure 1. Study area: the Marvdahst Plain, Fars Province and its annual average precipitations from 1990 to 2017 (Sources: IMO, 2018)

2.2 Sentinel-2 and Landsat-8 imagery

This study has required a double dataset of images: monthly Sentinel-2 images for crop mapping in spring (images from January to June) and summer (July to December) 2018 and monthly Landsat-8 imagery over the same year for crop water needs according to PYSEBAL inputs requisites (Figure 2). First, 11 Sentinels-2 images were downloaded (images in February were too cloudy, therefore we computed the average between January and March NDVI) to assess the evolution of pixel's greenness throughout the season. The images were downloaded using the USGS Data Explorer (USGS, 2019). This evolution enabled to distinguish them according to crop types collected on the ground. A field survey was conducted across the Marvdasht plain during the agricultural season (January-August) in 2018. The aim was to record GPS-based locations of each crop type in spring and summer (Table 3). The crop calendars were extracted from interviews with 60 farmers and also from NDVI temporal profiles of sampled crop types (based on Table 1).

Table.1 Sampled crop types and land uses in Marvdasht plain during the field work in 2018 (January-August)

Spring	Alfalfa	Canola	Orchard	Wheat	Bare soil	Urban			
(534)	20	24	134	244	26	86			
Summer	**Alfalfa**	**Orchard**	**Corn**	**Rice**	**Sugar beet**	**Tomato**	**Fallow**	**Bare soil**	**Urban**
(719)	20	134	60	174	100	79	40	26	86

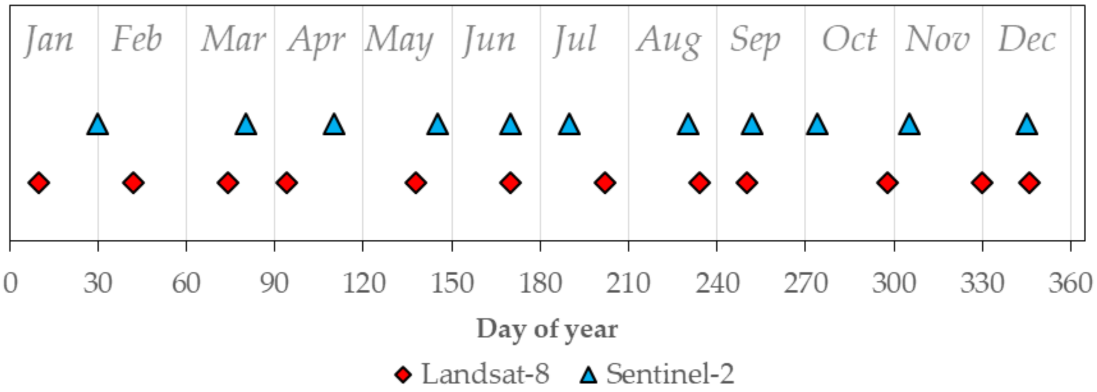

Figure.2 Timefarme of Landsat-8 and Sentinel-2 images for assessing crop water needs and crop mapping in Marvdasht, 2018

On each 'Day Of Year' timeframe, hourly ground data from an indicative station – Sad Doroudzan (X: 30,17, Y: 52,78, Z:1 600) (Figure 3) – were acquired to compute an instantaneous ET (ET_{inst}), during the time of overpass (11:00 GMT): solar radiation, wind speed, temperature and relative humidity (Figure 3). Sad Doroudzan station in Marvdasht plain was chosen as the reference station due to its proximity to fields and daily data recordings. PYSEBAL computes ET with a Standardized Penman-Monteith equation (Waters et al., 2002).

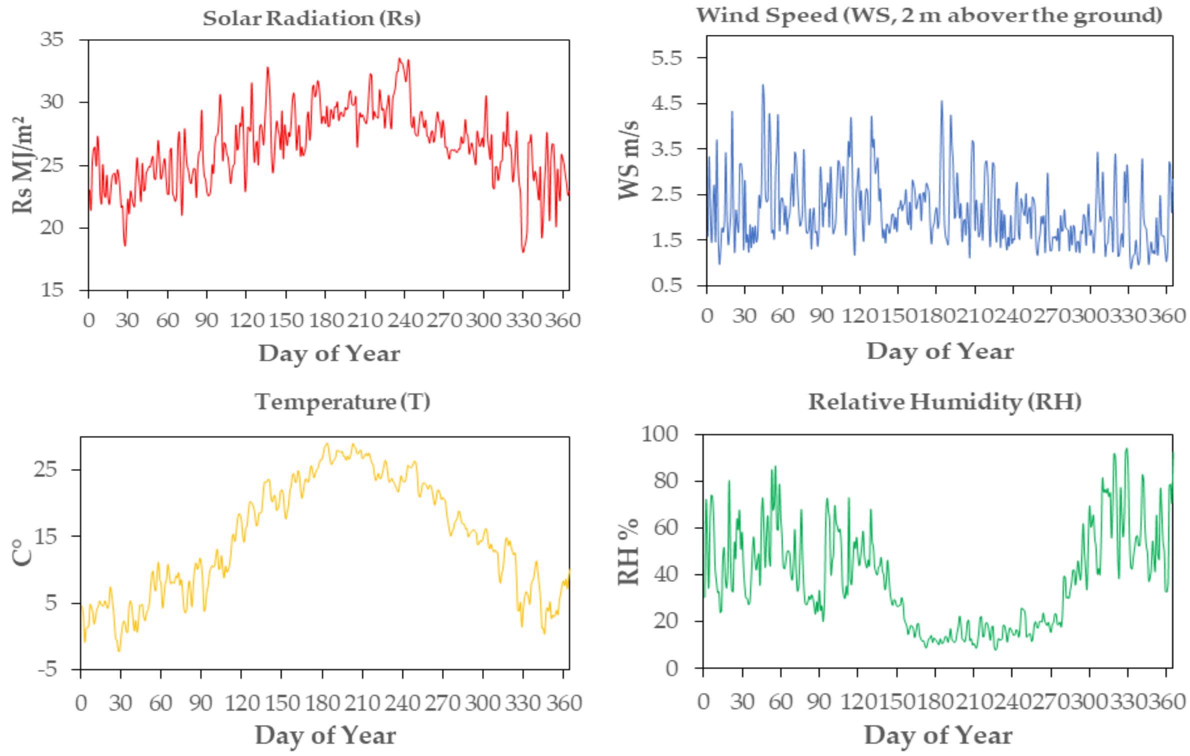

Figure.3 Daily ground data from Sad Doroudzan station for ET_{inst} estimation in PYSEBAL model in 2018

2.3. Crop mapping

Before any classification, the cultivated areas needed to be retrieved from satelite images without manual digitizing. We employed Normalized Difference Vegetation Index on Sentinel-2 images (NDVI) to delineate fields boundaries. The cultivated areas had a high NDVI (over 0.3) from March to November. The selection of these areas with the *Raster Calculator* in Arcmap (version 10.5.1) on each image, the polygonisation of these green areas and the stack of the monthly boundaries gave a final map of field boundaries.

From the sampled fields and crop types, the evolution of NDVI temporal profiles was extracted to differentiate crops calendar. The average of NDVI within the sampled fields were used to construct crops NDVI profiles (Figure 4).

Then, the crop type of unknown pixels needed to be classified. For this purpose, the NDVI profiles of all the previously delimited fields were computed and compared to the NDVI profiles from sampled fields. To conduct this comparison, the Euclidean Distance (ED) was computed (equation 1).

$$ED = \sqrt{\sum_{i=1}^{n}(a-b)^2} \qquad \text{Equation (1)}$$

Where a is the NDVI average of sampled fields and b, the unknown NDVI profiles to classify. n, is the number of month from the begining until the end of the season, depending on crop

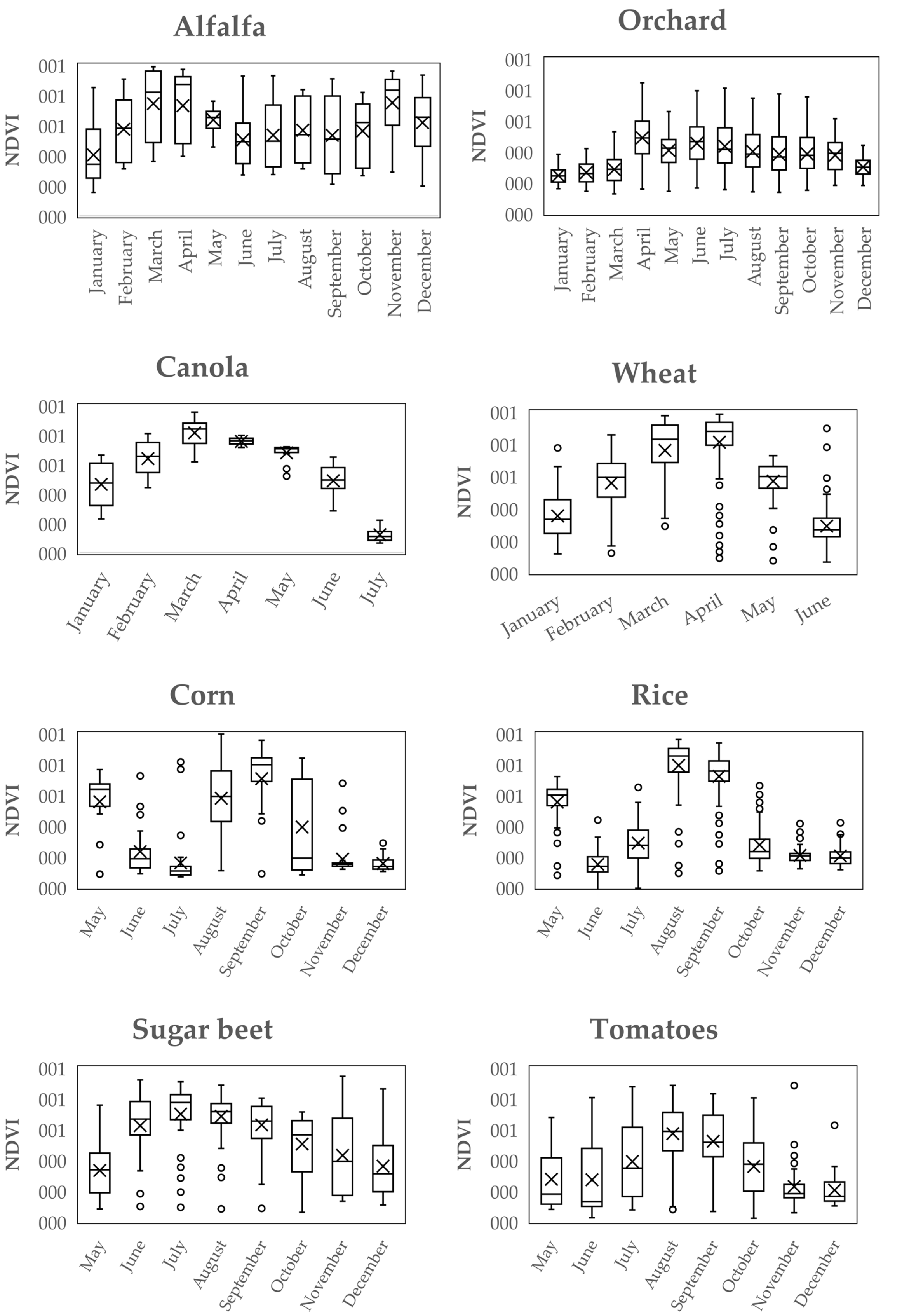

Figure.4 Sentinel-2 NDVI profiles of crop types and landuses from sampled fields in Marvdasht plain in 2018

types. When the ED is close to 0, the unknow NDVI profiles is considered as the crop type from the NDVI average of sampled fields. According to the results, a value of 0.4 was used as a threshold to define how close to 0 the ED was. If the ED classification could not find any crop type, our research classified the pixel as “spring vegetables” since there were numerous fields of garlic, carrots, onions or other vegetables according to fields observations. Contaminated pixels on the limits of the fields were removed by splitting fields with roads map, digitalized from *GoogleEarth* images, with a broad buffer which separates every field (roads and ditches).

The last step was the validation of the classification. This was computed by using the sampled and known fields. They were classed into two equal groups: known fields and false unknown fields. For instance for wheat, the 244 known fields were divided into two groups of 122. The first 122 were used to compute the NDVI profile of wheat (crop calendar) and the other 122 were tested for classification according to ED to the first group. The outputs of this validation are presented in the results.

2.4. PYSEBAL ET_{season} and NIR_{season}

PYSEBAL estimates the transfer of energy from the solar radiation to the water transfer to the atmosphere. This transfer can be quantified with the estimation of crop evapotranspiration (ET) and PYSEBAL requires the calculation of ET reference (ET_0) from ground datasets. In Marvdasht, previous studies on rice evapotranspiration suggested using the equation of Hargreaves-Samani (Fooladmand et al., 2008, 2008) for its accuracy in semi-arid climates. The equation of ET0 is written as follows (equation 2):

$$ET_0 = 0.00256 * (T_{mean} + 17.8) * (T_{max} - T_{min})^{0.5} Ra \qquad \text{Equation (2)}$$

Where T_{mean} is the daily average temperature, T_{max} and T_{min} are the maximum and minimum temperature during the day. Ra is the daily extraterrestrial radiation (MJ/m²/day) and assesses the income radiation to the atmosphere. Ra is obtained from the original FAO equation (FAO, 1986):

$$R_a = \frac{24*60}{\pi} G_{sc}\, d_r\, [\omega_s \sin(\varphi) \sin(\delta) + cos(\varphi) \cos(\delta) \sin(\omega_s)] \qquad \text{Equation (3)}$$

Where G_{sc} is the solar constant 0.0820 MJ/m²/min, d_r the inverse relative distance Earth-Sun, ω_s the solar angle and φ the radian latitude. Once the data have been compiled (ET_0, Landsat-8 images, Solar radiation, Wind speed, Temperature and Relative humidity), one can run the new version of PYSEBAL: PYSEBAL 3.4.0.0 (Hessel et al., 2017). ET_{inst} is first processed from the Latent Heat Flux (λET), based on the subtraction of Net Radiation (Rn), Soil Heat Flux (G) and Sensible Heat Flux (H): λET will be later converted into an amount of evaporated water, calibrated with the ET_0 from the station.

$$\lambda ET = R_n - G - H \qquad \text{Equation (4)}$$

The overall steps of PYSEBAL are summed up in a flowchart (Figure 5).

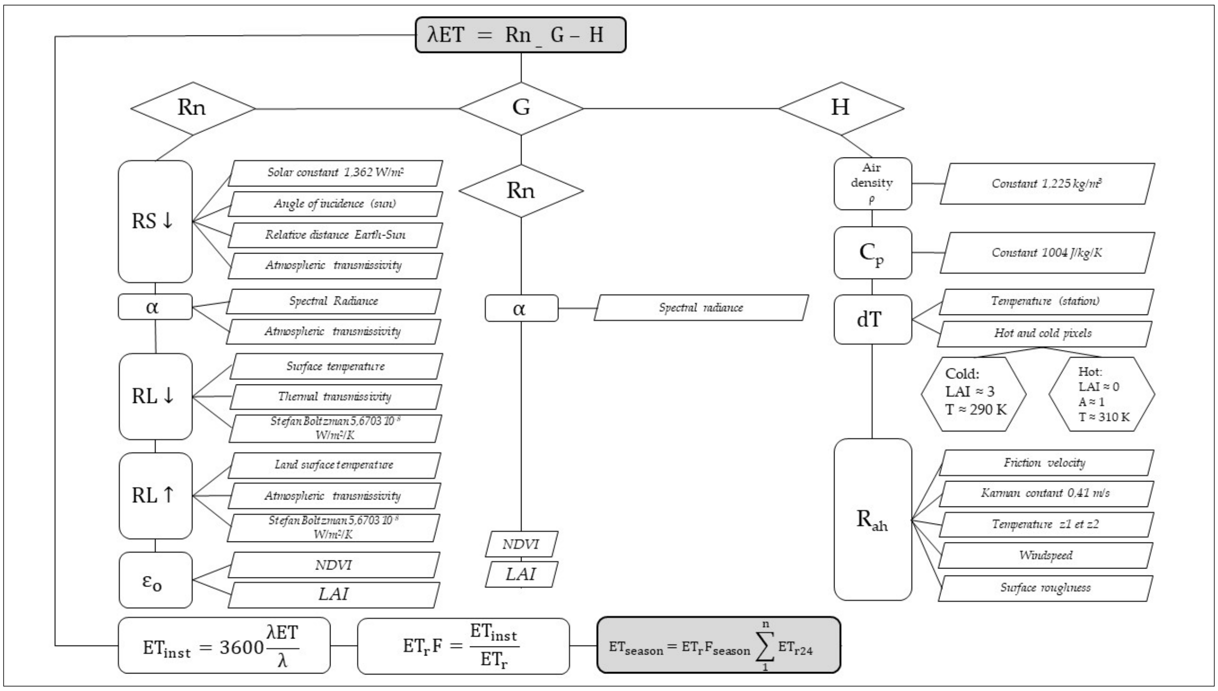

Figure.5 Flowchart of PYSEBAL, modified after Waters et al., 2002

R_n (W/m²) is the result of the subtraction of all of the outcoming radiation (through reflection) to all of the incoming radiations (long and shortwaves):

$$R_n = \mathrm{RS}\downarrow - \alpha\,\mathrm{RS}\downarrow + \mathrm{RL}\downarrow - \mathrm{RL}\uparrow - (1-\varepsilon_o)\mathrm{RL}\downarrow \qquad \text{Equation (5)}$$

Where $RS\downarrow$ matches to the shortwave incoming radiation in W/m² estimated from the solar constant (the theoretical amount of solar energy on 1 m²), the relative distance Earth-Sun and the atmospheric transmissivity which describes the transparency of the atmosphere, α is the surface albedo (the reflected fraction of sunlight from the Earth surface, written by Waters (Waters et al., 2002) and ε_o, thermal emissivity in W/m.

Second, RL↓ (the incoming longwave radiation) is estimated from T_a the near-surface air temperature at the station (in Kelvin, K), ε_a the atmospheric emissivity derived from the atmospheric transmissivity with a coefficient of 0.85 (Hessel et al., 2017; Waters et al., 2002), and σ, the content of Stefan-Boltzmann to describe reflected energy from a black body on the ground (5.67×10^{-8} W/m²/K):

$$\mathrm{RL}\downarrow = \varepsilon_a \times \sigma \times T_a^{\,4} \qquad \text{Equation (6)}$$

Comparably, RL↑ equation uses T_s the surface temperature instead of T_a (K). Waters *et al.*, (2002) suggested to compute surface temperature using the first band thermal (band 10) and the K_1 (774.8853) and K_2 (1321.0789) constants of each image. The corrected thermal radiance from the surface is estimated with the equation of Wukelikc (Wukelic et al., 1989) using the spectral radiance of band 6 to convert Digital Numbers (DN) to Radiance.

Once R_n has been computed, one can proceed with the Soil Heat Flux (G) in W/m², defined as a ratio with R_n:

$$G/R_n = Ts/\alpha\,(0.0038\alpha + 0.0074\alpha^2)(1 - 0.98\mathrm{NDVI}^4) \qquad \text{Equation (7)}$$

The multiplication of this ratio with R_n gives G. Second, the Sensible Heat Flux (H) in W/m² is assessed by equation 17. This step is the most complex since it uses some ground data which must be correctly recorded. In addition, one needs to select the hot and cold pixels to compute H (selection according to criteria table 2), which determines the quality of the outputs.

$$H = (\rho \times c_p \times dT) / r_{ah} \qquad \text{Equation (8)}$$

Where ρ is the air density (1.225 kg/m³), c_p the amount of heat required to change the temperature of 1C° (1004 J/kg/K), dT the temperature difference between two heights (z_1 : 0.1 m and z_2 : 2 m above surface) and r_{ah} the aerodynamic resistance to heat transport in s/m (the heat and vapour transfer from the surface to the edge of the canopy) under the influence of wind speed (from Sad Doroudzan) and surface roughness using NDVI and albedo in PYSEBAL. The definition of temperature at 2 m of height must be computed with indicative pixels: cold and hot.

Table.2 Criteria which wereused to select hot and cold pixels in PYSEBAL

	Criteria	Values	Purpose	Remarks
Cold pixels	LAI	4 - 6	Delineate a threshold of ET on the most well-watered pixels, where ET is the highest.	Cold pixels excluded water bodies where there was no transpiration. Thereby, pixels covered by well-irrigated vegetation were selected.
	NDVI	NDVI_{max}-0.1xNDVI_{std}		
	T_s	284 - 295 K		
	albedo	0.22 – 0.24		
	Elevation range	1400 - 1800	Removing the mountainous areas	

	Criteria	Values	Purpose	Remarks
hot pixels	LAI	0 – 0.4	Delineate a threshold of ET on the less well-watered pixels, where ET is the lowest	Dry fields with a weak vegetation coverage were favoured. Transpiration and evaporation would be low, but not null. Hot pixels did no cover deserts since the surface temperature was too high
	NDVI	0.03 – 0.20		
	T_s	302 - 310 K		
	albedo	0.13 – 0.15		
	Elevation range	1400 - 1800	Removing the mountainous areas	

Once R_n, G and H were computed, thenλET (equation 8) could be calculated. The latent heat flux is converted in an amount of ET at the time of Landsat-8 overpass:

$$ET_{inst} = 3600\,\frac{\lambda ET}{\lambda} \qquad \text{Equation (9)}$$

The conversion from second to the hour is necessary to compute the hourly ET when the satellite overpasses the plain. λ is the necessary latent heat to change a kilo of water from liquid to gaseous state (326.508 J/kg). The ratio between ET_{inst} from PYSEBAL and the ET_0 from the Sad Doroudzan (when Landsat-8 overpasses) is expressed as follows:

$$\mathrm{ET_rF} = \frac{\mathrm{ET_{inst}}}{\mathrm{ET0}}$$ Equation (10)

Where ET_rF is named ET fraction. ET_rF values are close to crop coefficients and enable to calibrate ET to different crop in the next equation (Waters et al., 2002). This ratio of ET_rF is then used to calibrate the daily ET_0 of Sad Doroudzan over the whole seasons (the length depends on the crop calendars of each crop). Since ET_0 to the station is available every hour of the season, the ration between ET_{inst} and ET_r can be calculated on each image and converted into a seasonal ET of several months:

$$\mathrm{ET_{season}} = \mathrm{ET_rF_{season}} \sum_1^n \mathrm{ET_{r24}}$$ Equation (11)

Where ET_rF_{season} is ET_rF within the season of one crop or another and $\sum_1^n ET_{r24}$, the sum of daily ET_r over the season. In order to delineate the beginning and the end of the season, PYSEBAL recommends to retain the first day of the first month of the season of wheat for instance and the last day of the last month. Ground data of Sad Doroudzan on the day pass of Landsat-8 are necessary to interpolate ET_{inst} to the all plain. The sum of ET_{24} gives the total evapotranspiration of crops (ET_{season}). For each crop areas, the average, the minimum and the maximum of ET are computed inside the fields polygons using *Zonal Statistics* from Qgis version 2.18.3.

Afterwards, the monthly and seasonal Net Irrigation Requirements (mm or m^3) can be estimated on each farm from the equation of the Food and Agriculture Organisation by the subtraction of ET and net rainfalls. Net rainfalls were computed with the CROPWAT software version 8.0 using *USDA Soil Conservation Service* methodology which requires precipitations as an input (Ewaid et al., 2019):

$$P_{net} = \frac{(\mathrm{P}*(125-0{,}2*3*\mathrm{P}))}{125} \quad \text{for } P <= \frac{250}{3}$$ Equation (12)

$$P_{net} = \frac{125}{3} + 0{,}1 * P \quad \text{for P} > \frac{250}{3}$$ Equation (13)

Were P_{net} is the effective rainfalls and P, the seasonal precipitations recorded in Doroudzan station in 2018 (in mm). And NIR equation:

$$\mathrm{NIR_{season}} = \mathrm{ET_{season}} - \mathrm{P_{net\_season}}$$ Equation (14)

The calculation of NIR_{season} for rice is somewhat different. Indeed, in the FAO method (Brouwer et al., 2001), rice is an exception to the ET-P_{net} equation. Irrigation inputs for rice are calculated with the following equation (15). The root zone of the rice is saturated during the sowing period with an initial supply of 200 mm (SAT). Then farmers apply a 100 mm water layer to keep the seedlings in water (WL). Finally, to compensate for the water lost through percolation in the soil, a daily supply of several mm of water is needed to ensure soil water saturation (PERC). This percolation has already been calculated and recorded with lysimeter data in the Marvdasht plain (Pirmoradian et al., 2002) and is measured at 3.4 mm/day for 4 months due to the fine-textured alluvial soils in the area. We, therefore, used this study as a reference to calculate the water requirement of rice and this value to compute PERC on our same study area.

2.5 Crop classification validation

It was necessary to assess the accuracy of the farm boundaries delineation through the comparison of areas from 60 automatically extracted and manually digitized fields with *GoogleEarth* images. R and R^2 were calculated to assess the reliability of the fields boundaries extraction. Once the farm boundaries are validated, the classification itself should be assessed with the computation of precision, recall and overall accuracy.

2.6 Crop water needs validation

The key point of this research was the validation of PYSEBAL outputs through the comparison of $NIR_{PYSEBAL}$ and NIR from the field surveys with farmers. The surveys targeted information about the yields and whenever possible, the irrigation calendar. More importantly, the surveys aimed to target the amount of irrigated water on crops. Whenever farmers knew the amount of irrigation they applied on their farms, we took the GPS coordinates and compared the Net Irrigation Requirements (NIR) from the surveys on these fields to the NIR of PYSEBAL on the same fields. These information collected from farmers might be incorrect or incomplete. Consequently, not all of the 60 surveys were retained as accurate and relaible enough to validate the NIR. However, a group of 5 farmers wrote down and precisely knew these information (times and volume) that were used to validate $NIR_{PYSEBAL}$: three fields of wheat, one of alfalfa and one of corn. On the sampled plots (where farmers knew exactly the amount of irrigation water they brought), we located and estimated the cultivated surface with *GoogleEarth* images (1), we multiplied the frequency of irrigation (number of irrigation session) with the amount of irrigation water per session (m^3) and we obtained the NIR of these fields. Then, we compared NIR_{field} with $NIR_{PYSEBAL}$ on the same plot. PYSEBAL outputs match to the ET and then to the NIR/ha/season (after net rainfall subtraction) per pixel. Therefore, we compare NIR_{fields} and $NIR_{PYSEBAL}$ per ha and per season. Consequently, despite the lack of lysimeter data, the accuracy of $ET_{PYSEBAL}$ could be assessed in this study through the comparison of NIR_{field} and $NIR_{PYSEBAL}$.

This lack of lysimetric data led us to consider a second process to validate ET_{season} of PYSEBAL. Indeed, this difficulty of the lack of data collected on the ground has already been encountered in other studies that recommend comparing Daily ET of PYSEBAL with Daily ET of the FAO-56 method (Stancalie et al., 2010) using Allen's method (Allen et al., 1998). This method consists in calculating Daily ET by calibrating ET_0 of the climatic station representative of the plain – here the Doroudzan station – with the crop coefficients (Kc) taken from the literature. Crop coefficients are indeed not the same from one crop to another and vary over time according to the crop phenological stage. It is important to compare the results of PYSEBAL in the Marvdasht Plain only from plots large enough to match the spatial resolution of Landsat-8 images. Thus, selected plots in the Marvdasht Plain should be larger than 4 hectares (Tasumi, 2019). The accuracy of PYSEBAL was assessed by calculating Root Mean Square Error (RMSE) and Mean Average Error (MEA) between Daily ET FAO-56 and the Daily PYSEBAL average of plots larger than 4 ha.

3. Results

3.1 Crop classification accuracy

Regarding the farm boundaries, with R: 0.95 and R^2: 0.91 (Figure 6), one can consider the model as accurate enough and these automated fields limits can be further used for crop areas classification. Also, the crop classification accuracy was estimated based on data…….. (Table 3).

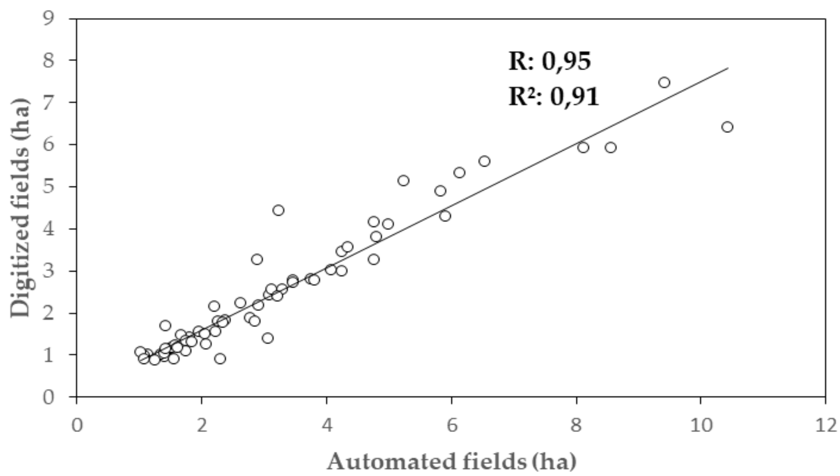

Figure.6 Comparison of automated and digitized farm boundaries in 60 random plots in Marvdasht plain

Table 3. Validation of crop areas classification in Marvdahst plain, 2018

(spring)	Precision	Recall	Overall accuracy	(summer)	Precision	Recall	Overall accuracy
Alfalfa	66.67	0.57	80	**Corn**	0.56	0.63	80
Canola	69.23	0.6	75	**Rice**	0.73	0.98	73.56
Orchard	93.75	0.94	89.55	**Sugar beet**	0.84	0.79	84
Wheat	98.1	0.94	84.43	**Tomato**	0.86	0.97	82.05
Urban	100	1	100	**Fallow**	0.9	1	90
Bare soil	81.25	0.81	100				

From spring to summer, the minimal overall accuracy is 73.56% (rice), the minimal recall 0.57 (alfalfa) and the minimal precision 0.56 (corn). In addition, rice and corn could be mixed up for their very similar crop calendars. Nonetheless, higher NDVI values of rice at mid-summer (figure 4) enabled the distinction of these two crop types. Otherwise, the classification of crop areas appeared as accurate enough to be used to compute the crop and eventually the total water budget in Marvdasht plain.

Crop mapping can be improved, as showed in the previous case of study that used this methodology with Sentinel-2 images (Caiserman et al., 2019). In this study, it was assumed that a greater number of GPS-based points per crop types (for crop calendars extraction) would enhance the accuracy of maps. Thereby, this paper showed that crops with similar agricultural calendars remain difficult to be distinguished, but the precision, recall and overall accuracy of the crop maps in Marvdasht plain were still satisfying and make these maps convenient for crop water needs estimations.

3.2 PYSEBAL's results accuracy

In most of the cases, PYSEBAL underestimates the reality with an average of 10% (table 4). The best estimation is the plot n°4 (wheat) where PYSEBAL only underestimated the reality of 1.96%. The statements of the farmers and PYSEBAL outputs were highly correlated. On the other hand, the worst example was another wheat field (overestimation of 17%) where $NIR_{PYSEBAL}$ was 459 mm/ha/season and NIR_{fields}, 384 mm. This might be due to errors from the farmers who probably underestimated the amount of irrigated water. The pixels of the outputs could be also overlapped with other fields and the estimation not accurate. Nonetheless, the overall estimation is satisfying and PYSEBAL is therefore considered as reliable enough to compute crop water needs.

Table.4 Comparison of $NIR_{PYSEBAL}$ and NIR_{fields} from the agricultural season in Marvdasht (2018)

Plot n°	Crop type	X	Y	Area	Frequency	Amount m³	NIR_{fields} mm/ha	$NIR_{PYSEBAL}$ mm/ha	Over/under-estimation of NIR (%)
1	Alfalfa	52.84	29.84	2.443	15	95	1425	1343	-5.92
2	Corn	52.80	29.93	2.294	6	86.4	518	473	-9.08
3	Wheat	52.79	29.93	1.418	4	86.4	346	268	-25.4
4	Wheat	52.84	29.84	1.395	4	90	360	353	-1.96
5	Wheat	52.84	29.84	3.513	4	96	384	459	17.70

Moreover, the comparison between Daily ET FAO-56 and PYSEBAL confirms the underestimation of PYSEBAL in most cases (Table 5, Figure 7). Indeed, all Daily ET PYSEBAL values are lower than those of Daily ET FAO-56 except for orchards due to a wider range of ET PYSEBAL average on account on the variety of fruit trees species in that class. The number of plots compared by crop type varied according to the importance of the plants. For example, only 12 plots of canola larger than 4 ha were compared as canola is only marginally grown in the plain, compared to 917 plots of wheat, a major crop in the plain. In total, the RMSE between

ET Daily FAO-56 and PYSEBAL was 0.67 mm/day and the MAE 0.52 mm/day. One must take into account the bias of the FAO-56 method (Allen et al., 1998), which only considers well-irrigated plots with no water deficit, which is not necessarily the case for all the plots compared in Table 5. However, despite the lack of expensive and scarce lysimetric data in the field, the relatively low values show the relative accuracy of PYSEBAL in its estimate of Daily ET in 2018 in the Marvdasht Plain.

Table.5 Crop coefficients retrived from the literature for FAO-56 method and Daily ET from FAO-56 and PYSEBAL in Marvdasht plain in 2018

Crops	Kc_{in}	Kc_{mid}	Kc_{end}	Length (days)	Plots over 4 ha	FAO-56 Daily ET	PYSEBAL Daily ET
Alfalfa	0.4	0.95	0.9	60	35	1.72	1.33
Canola	0.35	1.15	0.35	175	12	3.02	2.99
Orchard	0.4	1.1	0.45	150	57	3.43	3.61
Wheat	0.3	1.15	0.32	240	917	1.96	1.78
Corn	0.3	1.2	0.75	150	267	5.49	4.17
Rice	1.05	1.2	0.75	150	60	7.13	6.17
Sugar beet	0.35	1.2	0.7	160	122	6.10	5.74
Tomato	0.6	1.15	0.8	140	167	4.73	3.94

Figure.7 Comparaison of Daily ET FAO-56 and Daily ET PYSEBAL in the Marvdasht plain in 2018

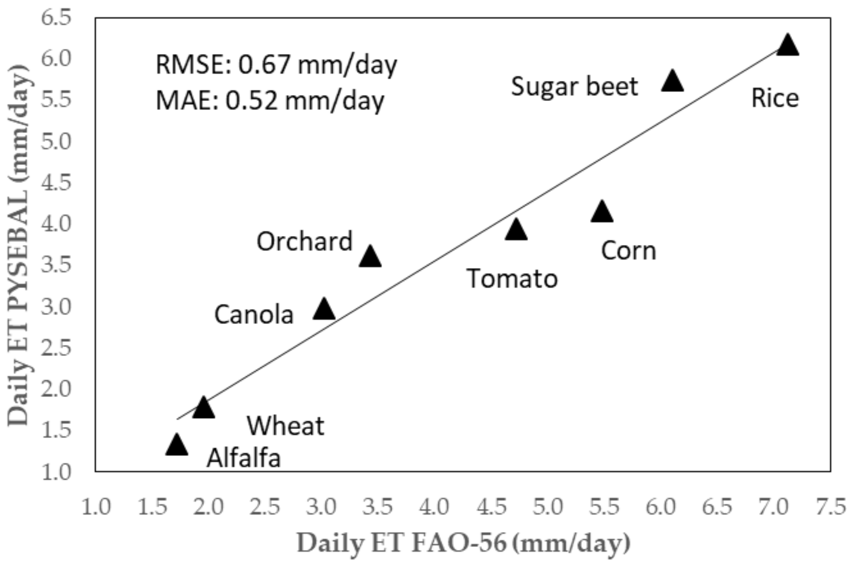

3.3. Water balance of Marvdasht plain

The results of the crop classification provide an agricultural census of Marvdasht plain in 2018. Table 6 shows the areas per crop type and Figures 8 and 9 locate each plot per crop type. In spring, over 32250 ha was cultivated, mostly wheat (17811 ha, 50.5% of the plain, Figure 8), as one of the key crops for food security and self-sufficiency in Iran. Rice is also a key-crop for food security and is intensively cultivated in Marvdasht. It is a traditional crop, especially in the northern part of the plain, but the construction of a dam in Doroudzan with a maximum capacity of one billion m^3 (Figures 8 and 9) in the 1970s drastically increased the area of rice, as another key crop of food security in Iran (Moameni, 1999). Rice cultivation had become almost industrial and remains as one of the most profitable crops in this region. Summer vegetables are exclusively composed of tomatoes and sugar beets on mid-areas, 12.8 and 8.6%, respectively. Overall, the crop choices in Marvdasht are not too diverse and follow clear trends of food production within a legitimate food security perspective.

Table.6 Spring and summer crop areas in Marvdasht plain based on crop classification with Sentinel-2 images in 2018

Crops (spring)	Area (ha)	Area (%)	Crops (summer)	Area (ha)	Area (%)
Wheat	17811	50.5	Corn	7184	22.2
Spring vegetable	14014	39.8	Rice	5433	16.8
Orchard	1818	5.2	Tomato	4140	12.8
Alfalfa	1548	4.4	Sugar beet	2768	8.6
Canola	59	0.2	Orchard	1818	5.6
Total	35250	100	Alfalfa	1548	4.8
			Total	32307	100

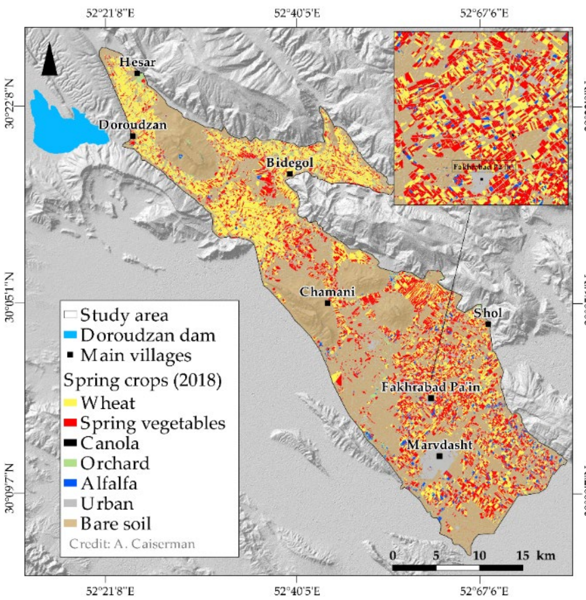

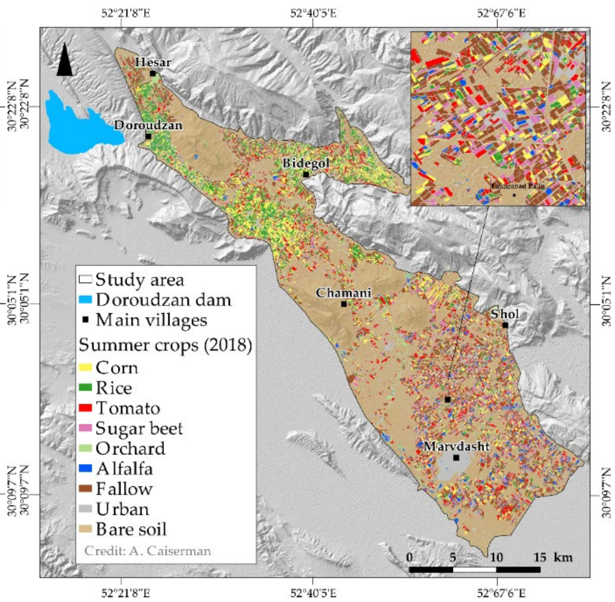

Figure 8. Crop map in spring 2018 **Figure 9.** Crop map in summer 2018

The map (Figure 10) shows the seasonal spatial distribution of the PYSEBAL ET_{season} and Table 7 shows the water balance information for the Marvdasht Plain. Firstly, it appears that the plain is more intensively cultivated in spring than in summer due to respective rainfall of 181 mm and 119 mm. The results of PYSEBAL thus make it possible to calculate the total irrigation needs of the plain in 2018 (Table 7).

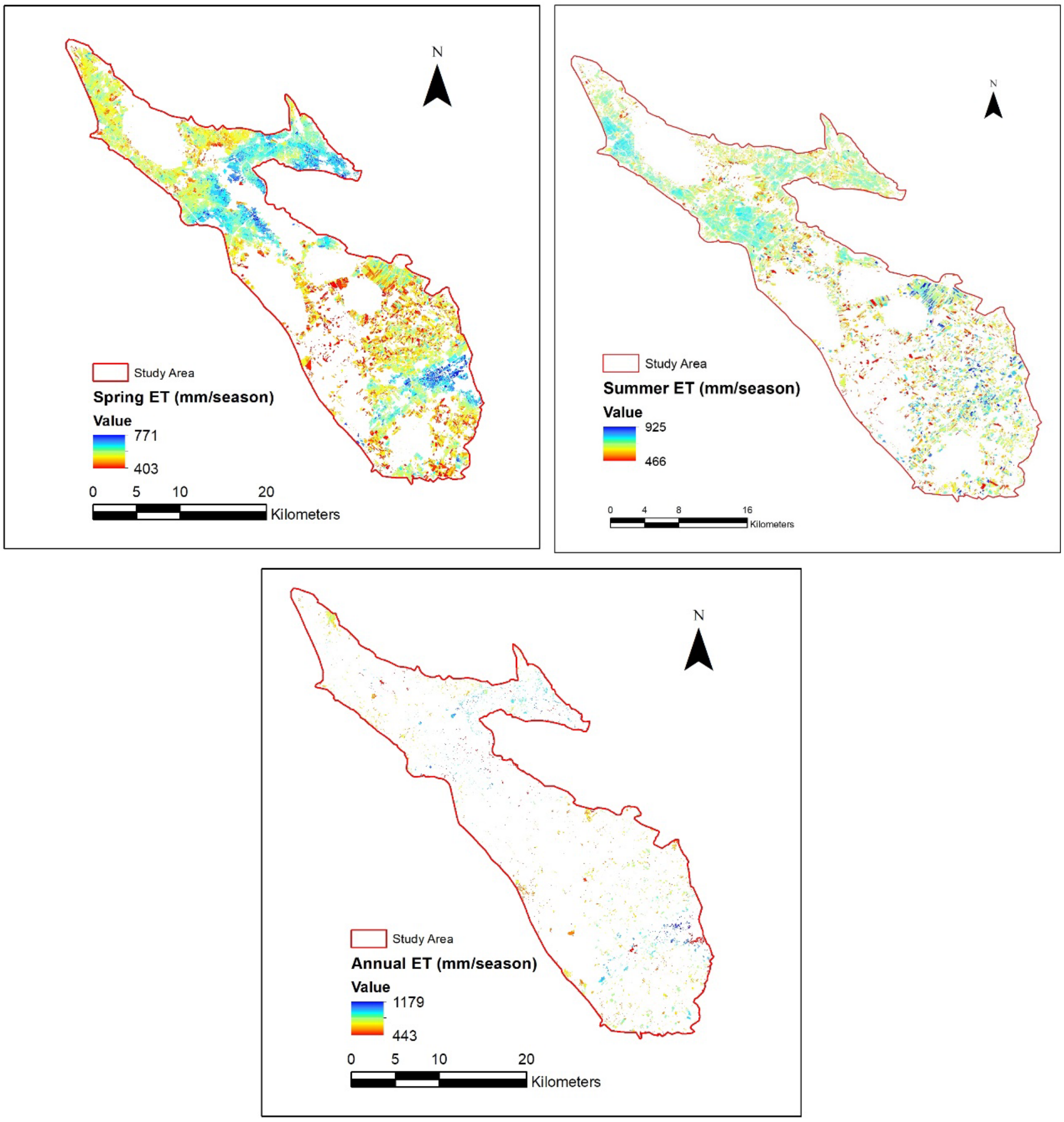

Figure 10. Maps of annual, spring and summer ETseason based on PYSEBAL in Marvdasht plain in 2018

The last column of Table 7 allows to prioritize the crops according to their pressures on the groundwater resource by dividing NIR_{season} of each crop with the volume precipitated and available for aquifer recharge on each surface. It is clear that rice exerts the greatest pressure because of its total irrigation needs. Indeed, the volume needed to irrigate all rice plots in 2018 was 11.92 times the volume of water available for groundwater recharge. Rice NIR_{season} was between 770 and 907 mm depending on the plots with NIR_{season} ranging from 1359 to 1496 mm according to Brouwer's equation (Brouwer et al., 2001). Rice is thus a crop that consumed too much water compared to the renewable water resource and therefore does not seem to be adapted to the water resource of this semi-arid context. On the other hand, all the plants that appear in red in Table 7 are in this same case of over-consumption of water to different degrees, from corn (pressure 5.61 times higher) to tomatoes (pressure 1.44 higher).

Table.7 Water balance from ET_{season} and NIR_{season} of the cultivated crops in the Marvdasht plain 2018

Crops	ET_{season} (mm/season)			$Net_{Rainfall}$ (mm/season) *	NIR_{season} (mm/season)			area (ha)	Total NIR (km^3)*	Total available precipitations for groundwater recharge (km^3)	Pressure on groundwater resource
	min	max	average		min	max	average				
Rice	770	907	839	119	1359	1496	1427	5433	0.0775	0.0065	11.9275
Corn	650	925	788	119	531	806	669	7184	0.0480	0.0085	5.6176
Sugar beet	780	841	811	164	616	677	647	2768	0.0179	0.0045	3.9421
Canola	525	771	648	181	344	590	467	59	0.0003	0.0001	2.5801
Alfalfa	841	1179	1010	332	509	847	678	1548	0.0105	0.0051	2.0422
Spr. veg.	403	682	543	181	222	501	362	14014	0.0507	0.0254	1.9972
Wheat	408	647	528	181	227	466	347	17811	0.0617	0.0322	1.9144
Tomato	466	615	541	221	245	394	320	4140	0.0132	0.0091	1.4457
Orchard	443	869	656	332	111	537	324	1818	0.0059	0.0060	0.9759
Total								**54775**	**0.2859**	**0.098**	

***Net rainfall** is the amount of net precipitation that occurred during the season of the matching crop.

Total NIR is the product of multiplying the average NIR_{season} with the cultivated area.

Total available precipitations is the volume of precipitations that occurred during the season and available for aquifer recharge

Pressure on groundwater resource is the number of times the NIR_{season} exceeded the matching $Net_{rainfall}$. This highlights the sensitive crops regarding water in this semi-arid plain.

In addition, these NIR_{season} values obtained with rice are lower than those obtained by lysimetric measurements in the Pirmoradian study (Pirmoradian et al., 2002): 1983 and 2361 mm/season, which confirms the underestimates of PYSEBAL. These plants, because of their surface areas and their ET_{season} and NIR_{season} are too large and the results of PYSEBAL allow us to identify the crops on which action should be taken either by reducing the cultivated areas or by improving irrigation techniques by adopting, for example, the drip or sprinkler systems which are very little present in the plain according to surveys with farmers. On the other hand, only the orchards have a water consumption adapted to the water available for recharging (pressure less than 1 in green in Table 7). Orchards benefit indeed from a more modest ET_{season} ranging from 443 to 869 but especially from a long rainy season (332 mm) as it is an annual crop. In theory, all the plants cultivated in the plain should have a NIR_{season} that is lower than the volume available for recharge. This negative water balance leads to a total groundwater consumption of 0.2859 km^3 for a precipitation volume available for recharge of only 0.098 km^3. If such water use is repeated every year, this water balance necessarily leads to a decrease in the piezometric level of the Marvdasht Plain. For this reason, we asked the 60 farmers in the surveys the current depth of their wells as well as the depth estimated some 30 years ago. According to these surveys, the average drawdown of the water tables would have been 125 m over the last thirty years due to the intense use of groundwater. This trend can only be confirmed by the negative water balance of PYSEBAL in 2018 and the intensive cultivation of these plants in the Marvdasht plain every year for the last 50 years or so, as already shown by Momeni's report in that study area twenty years ago (Moameni, 1999).

4. Discussion

4.1 PYSEBAL ET_{season} variabiliy

Table 7 reports some variability in ET_{season} and NIR_{season} proportionally, based on the net precipitation for each plant. We saw in the Hargreaves-Samani equation at Sad Doroudzan station that was used as a reference to calibrate ET_{inst} from PYSEBAL at 11:00 GMT each day took into account temperature and solar radiation while the Standardized Penman-Monteith equation used temperature, wind speed, radiation and relative humidity. We therefore compared Daily ET from Hargreaves-Samani with ET_r24 PYSEBAL on a grassy (assumed to be well watered) plot of 11 ha next to Sad Doroudzan station (figure 11). This comparison first explains the heterogeneity of PYSEBAL's results over the whole plain as PYSEBAL takes into account the calibration between two different equations in the calculation of ET_{season}: the reference equation at the station and the reference equation calculated by PYSEBAL.

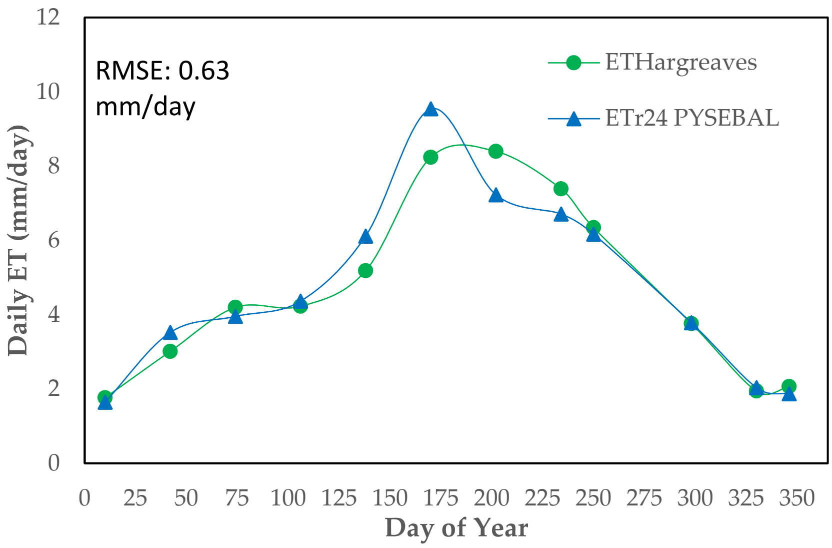

Figure 11. Comparison of Daily $ET_{Hargreaves}$ at Sad Doroudzan station and ET_r24 PYSEBAL

Indeed, the comparison of daily ET results shows some differences at the scale of the hydrological year. The RMSE is 0.63 mm/day and the MAE is 0.46 mm/day. The difference between the two ET is thus slight and ET_r24 estimated by PYSEBAL remains very close to the $ET_{Hargeaves}$ observed on the day of the Landsat-8 overpass. Only days 42 (March), 106 (May), 138 (June), 138 (July) and 170 (August) showed an overestimation of ET_r24 compared to the $ET_{Hargreaves}$ of the station. However, this slight difference may have consequences on the ET_{season} of the Marvasht Plain. Moreover, ET_{season} of PYSEBAL remains very dependent on the climatic data recorded at the Sad Doroudzan station. We calculated the correlation between ET_r24 of the nine largest and closest plots to the Sad Doroudzan station (one sample plot per crop type) and the daily climatic parameters used by PYSEBAL at the time of the Landsat-8 run: Relative Humidity, Temperature, Wind Speed and Radiation (Figure 12). There is a strong correlation between ET_r24 and RH with a minimum R^2 of 0.75 in Table 8, and Temperature ($R^2$2: 0.87) and Radiation (R^2: 0.86). Only the relationship between Wind Speed and ET_r24 seems weaker because Wind Speed can be very variable from one area to another and it seems that PYSEBAL minimizes the weight of WS in its estimate of ET_r24. Recall here that these correlations are such that they are for the plots closest to the reference station used in our case study. The variability of the ET_{season} by crop type on the plots closest to the station because the climatic data are homogeneous up to a certain radius. Indeed, the climatic conditions are not exactly the same between the north, the centre and the south of the plain. Logically, Relative Humidity is lower in the drier areas where Temperatures and Radiation are higher. The four climatic parameters were not available at other stations in the Marvdasht Plain. Nevertheless, we compared the PYSEBAL outputs on Daily Radiation from each satellite image as well as Daily Surface Temperature between three different locations. Indeed, we compared these parameters between the recorded data (regarding temperature, Air Temperature of the station at 2 meters as compared to Landsurface Tempreature of PYSEBAL) at Sad Doroudzan with a well-irrigated alfalfa plot close to the station (over a large area of 11 ha) with an alfalfa plot south of 8 ha and an alfalfa plot north of 5 ha (Figure 12).

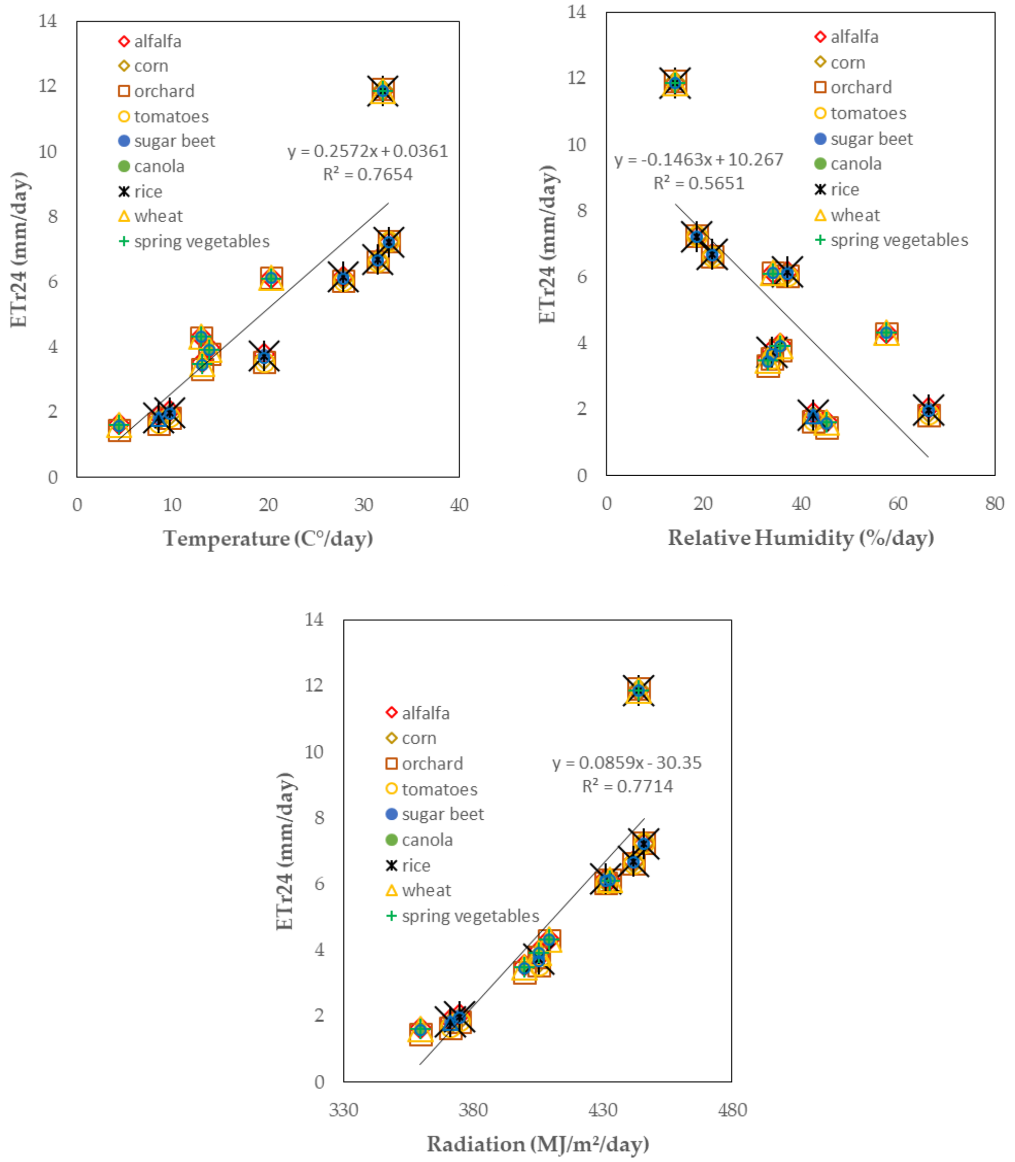

Figure 12. Strong potitive correlation between T (°C), RH (%), R (MJ/m²) and ET_r24 PYSEBAL

Table 8. R^2 between weather parameters and ET_r24 from PYSEBAL on sampled plots

Crops	T°	RH	Ws	R
alfalfa	0.88	-0.75	0.55	0.88
corn	0.87	-0.82	0.60	0.87
orchard	0.87	-0.75	0.55	0.88
tomato	0.99	-0.82	-0.32	0.99
sugar beet	0.87	-0.82	0.60	0.87
canola	0.98	-0.87	0.62	0.98
rice	0.87	-0.82	0.60	0.87

wheat	0.98	-0.76	0.82	0.86
spring vegetables	0.98	-0.76	0.82	0.86

Location near the station is 4 km to Sad Doroudzan, location south 55 km and location north 19 km. Logically, the daily temperatures at a location near the station are the closest to those recorded at Sad Doroudzan station. On the other hand, the further away from the station, the more different the temperatures are at location north (RMSE 7.2 Kelvin/day compared to Temperature at a location near the station) and south (RMSE 7.7 Kelvin/day compared to Temperature location near the station), which in this case are higher than the temperatures at a location near the station. The warmest surface temperatures are also located at the south location 55 km to the south, so a stronger ET_{season} can be expected (ET_{season} location near the station 1066 mm, south location: 1518 mm and north location: 1315 mm). Not all Surface Temperatures are the same everywhere, including in the PYSEBAL results, and ET_{season} will depend on this spatial distribution. On the other hand, the Radiation layer of PYSEBAL seems to be more homogeneous than the Surface Temperature layer (figure 14). Although ET_r24 was correlated with Radiation (Figure 13), it would appear that the Radiation does not vary much in the plain. However, the PYSEBAL Radiation of near, south and north locations records a high RMSE of 54 to 57 MJ/m^2/day which may limit the reliability of this layer at the scale of a whole plain, which is essential for the ET_{season} estimate.

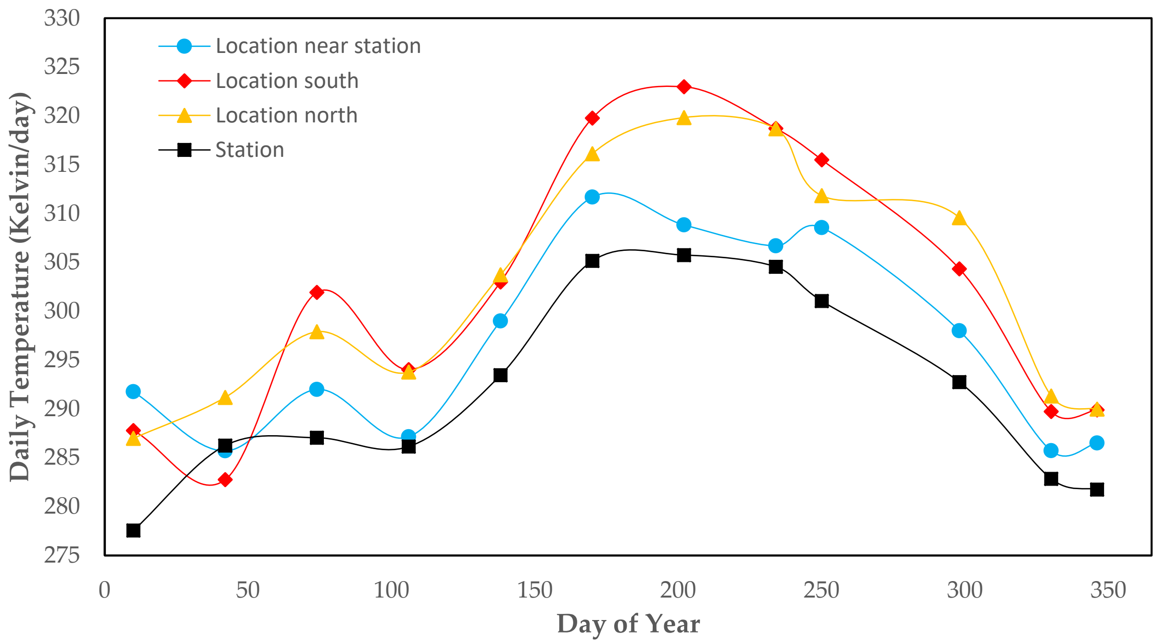

Figure 13. Comparison of 4 locations temperatures between observed air temperature data at Sad Doroudzan station and land surface temperature of 3 different locations in the plain

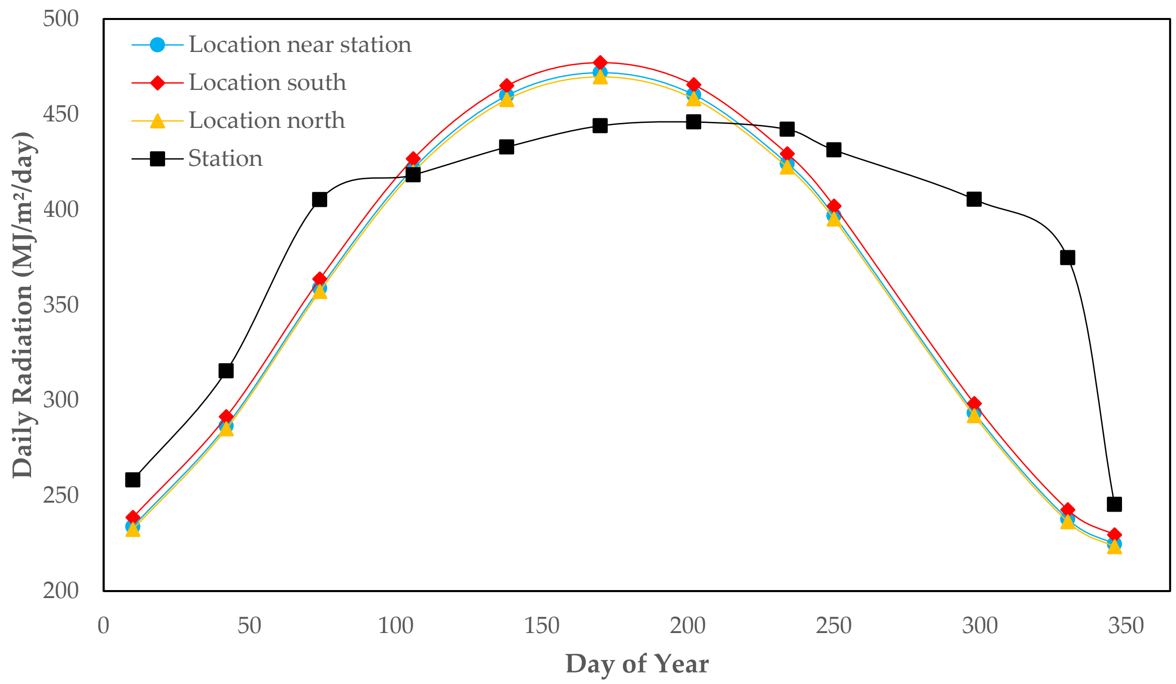

Figure 14. Comparison of 4 locations temperatures between observed air temperature data at Sad Doroudzan station and land surface temperature of 3 different locations in the plain

In the PYSEBAL results, Daily ET_r24 from the three alfalfa plots correlated well with both Surface Temperatures with a minimum R^2 of 0.57 and solar radiation with a minimum R^2 of 0.68 (Figure 15). This confirms the importance of climatic parameters in the variability of ET_{season} but also the fact that the variation comes more from the spatial distribution of Land Surface Temperature than from Radiation with which ET_r24. Indeed, if the whole plain was characterized by the same Surface Temperature on each Landsat-8 image for each day of passage, ET_{season} would probably record much smaller variabilities. This is a strength of the PYSEBAL model, whose spatial variations reflect different evapotranspiration realities over an entire plain.

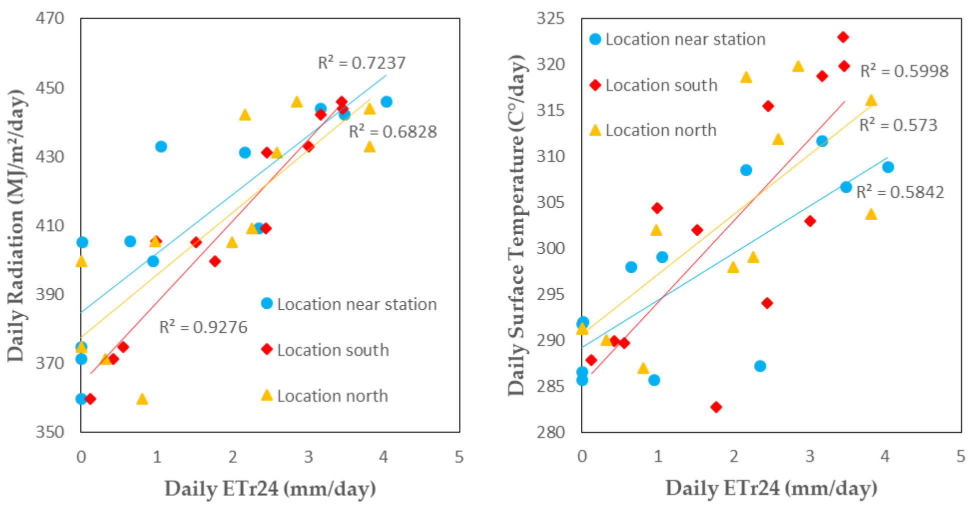

Figure 15. Strong positive correlation between ETr24 and PYSEBAL Land Surface Temperature and Radiation

We have just seen the reasons why ET_{season} recorded more or less significant variations in PYSEBAL's results. The predominance of climatic parameters is to be questioned in this variability but Table 7 on the water balance of the Marvdasht plain also showed the variability of the water used by the farmers, i.e. NIR_{season}. Although NIR_{season} is proportional to the ET_{season} in terms of available net precipitation, it would appear that there are other factors responsible for this variability.

4.2 NIR_{season} varability: groundwater economy

The Marvdasht Plain is also characterised by NIR_{season} variabilities. Although the soils in the region are predominantly fine-textured alluvial soils, the soil characteristics are important to consider. For example, the plots at the foot of the mountains are on deeper, sandier soils on which farmers will prefer to grow orchards rather than rice. Indeed, a rice plot on sandy soil would lead to higher percolation values than those obtained by lysimeters in the centre of the plain in previous studies (Pirmoradian et al., 2002). These values could thus reach 8 mm/day according to Brouwer (Brouwer et al., 2001), which would considerably increase the total percolation of the rice plot. However, beyond the soil conditions of the study area, farmers practices should be questioned, especially irrigation schedules and irrigation systems (Calera et al., 2017; Costa et al., 2019; Hess et al., 2016; Zwart and Bastiaanssen, 2007). For this purpose, we collected in the surveys the irrigation systems of 60 farmers. Of the 60 farmers surveyed, 52 use the furrow system which is more sensitive to evaporation. The variability of NIR_{season} can therefore be explained by this practice. Indeed, it would seem that the distribution of net rainfall varies very little between the north and the south of the plain. For example, the precipitation for the January-June period is 287 mm in the north of the plain and 272 mm in the south. Thus, we find wheat plots with low NIR_{season} of 227 mm/season in both the north and the south and NIR_{season} of 466 mm/season in both the north and the south. This means that some farmers irrigate more than their neighbours. This finding should put us on the track of the groundwater economy. Indeed, it would seem that farmers who irrigate more on their plots could apply smaller amounts of water, closer to those of their neighbours in the lower NIR_{season}. This shift from high NIR_{season} to low NIR_{season} can only be achieved by improving irrigation, starting with the amounts applied. Thus, we have estimated the groundwater savings that could be achieved in the plain if all farmers irrigated, theoretically, with the lowest NIR_{season} found in the plain (Figure 16).

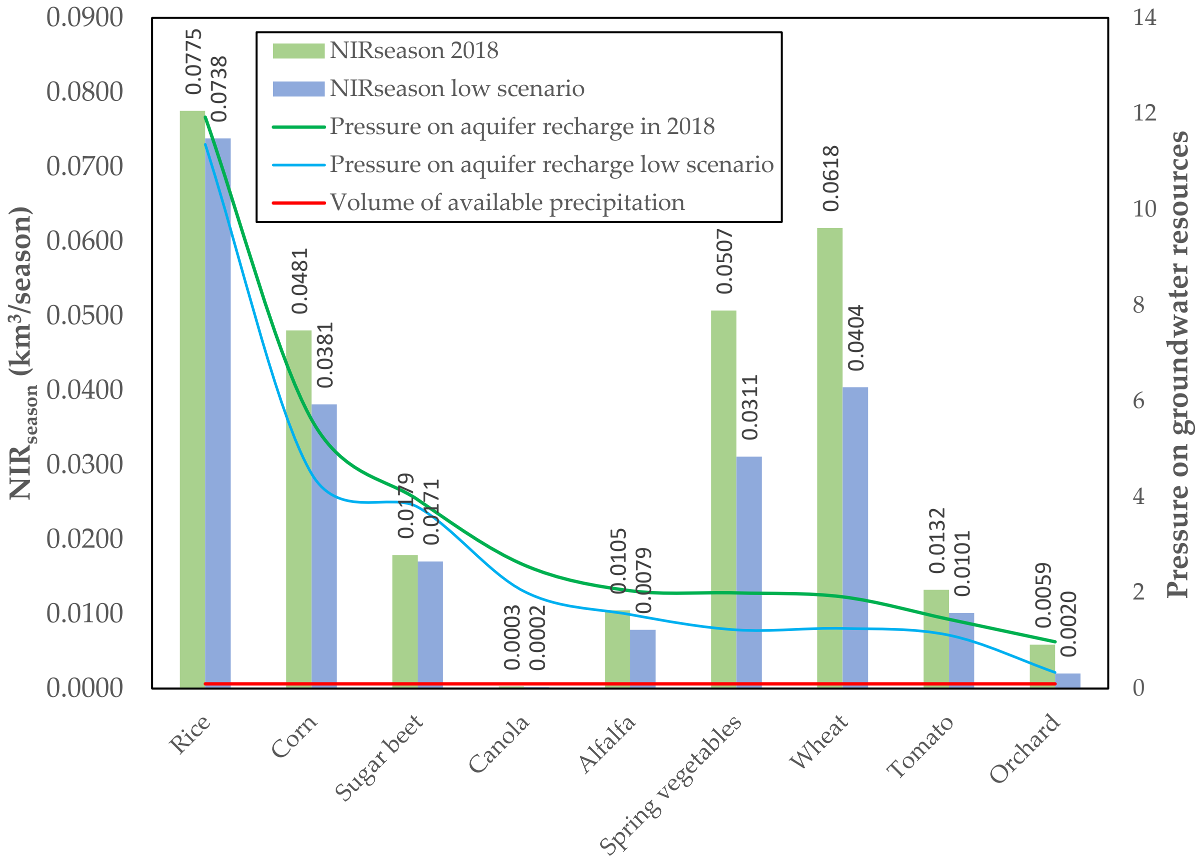

Figure 16. Possible groundwater economy in the Marvdasht plain in 2018

In this way, the pressure on water resources would be more modest than in the current context of the year 2018. Such a change would result in a total groundwater use of 0.2208 km^3 instead of the current 0.2859 km^3. In absolute terms, the water balance would have to become positive but this would imply drastic reductions in cultivated areas in addition to the adoption of lower NIR$_{season}$. However, this option does not seem to be economically feasible for farmers. However, even in this scenario, for all crops except orchards, the road to water savings is still long as NIR$_{season}$ remains higher than the volume available for aquifer recharge. This theoretical scenario is a true illustration of the usefulness of PYSEBAL in a water-saving objective, without reducing the cultivated areas. These results make it possible to set the objectives necessary to reduce water use in the Marvdasht plain.

5. Conclusion

This study showed the contributions of remote sensing to the estimation of the water balance of an important agricultural plain such as Marvdasht in southern Iran. This free technology requires some fieldwork, particularly for mapping crops from one season to the next. The fieldwork and NDVI classification mapping of each plot are largely dependent on agricultural calendars, but at the end of the agricultural year we showed that it was possible to map the plots quickly and with high accuracy. The second step, ET$_{season}$ estimation, can also only be done at the end of the crop year. PYSEBAL proved to be a relevant tool in the estimation of ET$_{season}$ and NIR$_{season}$. The validation of PYSEBAL with the field (comparison of NIR$_{PYSEBAL}$ and

NIR_{FIELD}) and with Daily ET FAO-56 was the biggest challenge of this study. PYSEBAL seems to underestimates the reality. Indeed, the lack of lysimetric data can limit the reliability of such models, but PYSEBAL seems robust in the case of Marvdasht as the differences between $NIR_{PYSEBAL}$ and NIR_{field}, and between Daily ET PYSEBAL et Daily ET FAO-56 remains low, and this study allowed to understand that the variability of ET_{season} came primarily from the variability of the Land Surface Temperature layer generated by PYSEBAL than from the Radiation Layer. Indeed, climatic conditions are not exactly homogeneous in all parts of an agricultural plain, which explains the heterogeneity of ET_{season} results. As such, the Radiation Layer, due to its homogeneity, does not seem to reflect this climatic diversity as much as the Land Surface Temperature layer.

Thanks to this methodological combination, it was possible to characterize crops according to their water requirements. Crops such as rice or maize have too high consumption in relation to the volume available for groundwater recharge. In this case, most of the crops had a negative water balance, which in 2018 led to the overutilisation of groundwater in the plain. Such practices can only lead to groundwater drawdown, but the advantage of this study is that it targeted the sensitive crops least adapted to the semi-arid context. In this respect, the results of this study are intended to be used by political decision-makers in the field of agriculture and water and are intended to be reproducible every year on any plain in the world. The variability of the NIR_{season} showed us that some farmers were able to irrigate less than their neighbours despite similar climatic conditions. It would seem that it is above all on practices that agricultural policies should act, in order to minimize the use of groundwater by tending towards these lower volumes already applied by some farmers.

References

Ahani, H., Kherad, M., Kousari, M.R., Rezaeian-Zadeh, M., Karampour, M.A., Ejraee, F., Kamali, S., 2012. An investigation of trends in precipitation volume for the last three decades in different regions of Fars province, Iran. Theoretical and Applied Climatology 109, 361–382.

Allen, G.R., Pereira, L.S., Raes, D., Smith, M., 1998. Crop evapotranspiration – Guidelines for computing crop water requirements. FAO, Rome, Italy.

Allen, R., Tasumi, M., Trezza, R., 2007. Satellite-Based Energy Balance for Mapping Evapotranspiration with Internalized Calibration (METRIC)—Model. Journal of Irrigation and Drainage Engineering 133, 380–394. https://doi.org/10.1061/(ASCE)0733-9437(2007)133:4(380)

Asgarian, A., Soffianian, A., Pourmanafi, S., 2016. Crop type mapping in a highly fragmented and heterogeneous agricultural landscape: A case of central Iran using multi-temporal Landsat 8 imagery. Computers and Electronics in Agriculture 127, 531–540. https://doi.org/10.1016/j.compag.2016.07.019

Attarod, P., Rostami, F., Dolatshahi, A., Sadeghi, S.M.M., Amiri, G.Z., Bayramzadeh, V., 2016. Do changes in meteorological parameters and evapotranspiration affect declining oak forests of Iran? Journal of Forest Science 62 (2016), 553–561. https://doi.org/10.17221/83/2016-JFS

Bastiaanssen, W.G.M., Menenti, M., Feddes, R.A., Holtslag, A.A.M., 1998a. A remote sensing surface energy balance algorithm for land (SEBAL). 1. Formulation. Journal of Hydrology 212–213, 198–212. https://doi.org/10.1016/S0022-1694(98)00253-4

Bastiaanssen, W.G.M., Pelgrum, H., Wang, J., Ma, Y., Moreno, J.F., Roerink, G.J., van der Wal, T., 1998b. A remote sensing surface energy balance algorithm for land (SEBAL).: Part 2: Validation. Journal of Hydrology 212–213, 213–229. https://doi.org/10.1016/S0022-1694(98)00254-6

Belgiu, M., Csillik, O., 2018. Sentinel-2 cropland mapping using pixel-based and object-based time-weighted dynamic time warping analysis. Remote Sensing of Environment 204, 509–523. https://doi.org/10.1016/j.rse.2017.10.005

Brouwer, C., Prins, K., Kay, M., Heibloem, M., 2001. Irrigation Water Management: Irrigation Methods. FAO, Wageningen, Netherlands.

Caiserman, A., Dumas, D., Bennafla, K., Faour, G., Amiraslani, F., 2019. Application of Remotely Sensed Imagery and Socioeconomic Surveys to Map Crop Choices in the Bekaa Valley (Lebanon). Agriculture 9, 57. https://doi.org/10.3390/agriculture9030057

Calera, A., Campos, I., Osann, A., D'Urso, G., Menenti, M., 2017. Remote Sensing for Crop Water Management: From ET Modelling to Services for the End Users. Sensors (Basel) 17. https://doi.org/10.3390/s17051104

Costa, J. de O., Coelho, R.D., Wolff, W., José, J.V., Folegatti, M.V., Ferraz, S.F. de B., Costa, J. de O., Coelho, R.D., Wolff, W., José, J.V., Folegatti, M.V., Ferraz, S.F. de B., 2019. Spatial variability of coffee plant water consumption based on the SEBAL algorithm. Scientia Agricola 76, 93–101. https://doi.org/10.1590/1678-992x-2017-0158

Ewaid, S.H., Abed, S.A., Al-Ansari, N., 2019. Crop Water Requirements and Irrigation Schedules for Some Major Crops in Southern Iraq. Water 11, 756. https://doi.org/10.3390/w11040756

FAO, 1986. Chapter 4: Irrigation water needs [WWW Document]. URL http://www.fao.org/docrep/S2022E/s2022e08.htm (accessed 8.4.18).

Faramarzi, M., 2010. Assessment of regional water endowments, crop water productivity, and implications for intra-country virtual water trade in Iran. University of Zurich, Zurich, Switzerland.

Fooladmand, H.R., Zandilak, H., Ravanan, M.H., 2008. Comparison of different types of Hargreaves equation for estimating monthly evapotranspiration in the south of Iran. Archives of Agronomy and Soil Science 54, 321–330. https://doi.org/10.1080/03650340701793603

Golian, S., Mazdiyasni, O., AghaKouchak, A., 2015. Trends in meteorological and agricultural droughts in Iran. Theor Appl Climatol 119, 679–688. https://doi.org/10.1007/s00704-014-1139-6

Hao, P., Tang, H., Chen, Z., Liu, Z., 2018. Early-season crop mapping using improved artificial immune network (IAIN) and Sentinel data. PeerJ 6. https://doi.org/10.7717/peerj.5431

Hassanshahi, H., Iravani, H., Daneshvar Ameri, Z., Kalantari, K., 2015. Measure and comparison of economic, social and ecological sustainability of farming systems in the Marvdasht plain. Desert 20, 231–239. https://doi.org/10.22059/jdesert.2015.56485

Hess, T., Daccache, A., Daneshkhah, A., Knox, J., 2016. Scale impacts on spatial variability in reference evapotranspiration. Hydrological Sciences Journal 61, 601–609. https://doi.org/10.1080/02626667.2015.1083105

Hessel, T., 2019. Add SEBAL. Contribute to wateraccounting/SEBAL development by creating an account on GitHub. Water Accounting.

Hessel, T., van Opstal, J., Trambauer, P., Mohamed, Y., Bastiaanssen, W., 2017. User Guide: pySEBAL for Landsat imagery (beta version). UNESCO - IHE, Delft, the Netherlands.

Heupel, K., Spengler, D., Itzerott, S., 2018. A Progressive Crop-Type Classification Using Multitemporal Remote Sensing Data and Phenological Information. PFG 86, 53–69. https://doi.org/10.1007/s41064-018-0050-7

Islamic Republic of Iran Meteorological Organisation, 2018. Climate data from Sad Doroudzan station. Tehran, Iran.

Karimi, V., Karami, E., Keshavarz, M., 2018. Climate change and agriculture: Impacts and adaptive responses in Iran. Journal of Integrative Agriculture 17, 1–15. https://doi.org/10.1016/S2095-3119(17)61794-5

Kenduiywo, B.K., Bargiel, D., Soergel, U., 2018. Crop-type mapping from a sequence of Sentinel 1 images. International Journal of Remote Sensing 39, 6383–6404. https://doi.org/10.1080/01431161.2018.1460503

Keshavarz, M., Karami, E., 2013. Institutional adaptation to drought: the case of Fars Agricultural Organization. J. Environ. Manage. 127, 61–68. https://doi.org/10.1016/j.jenvman.2013.04.032

Keshavarz, M., Karami, E., Zibaei, M., 2014. Adaptation of Iranian farmers to climate variability and change. Reg Environ Change 14, 1163–1174. https://doi.org/10.1007/s10113-013-0558-8

Khosravi, H., Sajedi Hosseini, F., Nasrollahi, M., Gharechaee, H.R., 2017. Trend analysis and detection of precipitation fluctuations in arid and semi-arid regions. Desert 22, 77–84. https://doi.org/10.22059/jdesert.2017.62173

Lamb, D.W., Brown, R.B., 2001. PA—Precision Agriculture: Remote-Sensing and Mapping of Weeds in Crops. Journal of Agricultural Engineering Research 78, 117–125. https://doi.org/10.1006/jaer.2000.0630

Liou, Y.-A., Kar, S.K., 2014. Evapotranspiration Estimation with Remote Sensing and Various Surface Energy Balance Algorithms—A Review. Energies 7, 2821–2849. https://doi.org/10.3390/en7052821

Madani, K., 2014. Water management in Iran: what is causing the looming crisis? J Environ Stud Sci 4, 315–328. https://doi.org/10.1007/s13412-014-0182-z

Madani, K., AghaKouchak, A., Mirchi, A., 2016. Iran's Socio-economic Drought: Challenges of a Water-Bankrupt Nation. Iranian Studies 49, 997–1016. https://doi.org/10.1080/00210862.2016.1259286

Menenti, M., Choudhury, B.J., 1993. Parameterization of land surface evaporation by means of location dependent potential evaporation and surface temperature range. Department for Environment, Food and Rural Affairs (Defra) 212, 561–568.

Moameni, A., 1999. Soil quality changes under long - term wheat cultivation in the Marvdasht plain, South - Central Iran. Ghent University, Ghent, Belgium.

Motamed, M., 2017. Developments in Iran's Agriculture Sector and Prospects for U.S. Trade. United States Depar tment of Agriculture, Washington D.C.

Neuve-Eglise, A., 2007. L'agriculture iranienne : une modernisation inachevée. La Revue de Téhéran.

Norman, J.M., Becker, F., 1995. Terminology in thermal infrared remote sensing of natural surfaces. Remote Sensing Reviews 12, 159–173. https://doi.org/10.1080/02757259509532284

Panigrahy, S., Sharma, S.A., 1997. Mapping of crop rotation using multidate Indian Remote Sensing Satellite digital data. ISPRS Journal of Photogrammetry and Remote Sensing 52, 85–91. https://doi.org/10.1016/S0924-2716(97)83003-1

Pirmoradian, N., Kamgar-Haghighi, A.A., Sepaskhah, A.R., 2002. Crop Coefficient and Water Requirement of Rice in Kooshkak Area, Fars Province. Journal Of Science And Technology Of Agriculture And Natural Resources 1, 10–22.

Roerink, G.J., Su, Z., Menenti, M., 2000. S-SEBI: A simple remote sensing algorithm to estimate the surface energy balance. Physics and Chemistry of the Earth, Part B: Hydrology, Oceans and Atmosphere 25, 147–157. https://doi.org/10.1016/S1464-1909(99)00128-8

Roshan, G., Negahban, S., 2015. Modeling of the effects of climate change on rainy and gully erosion potential of Kor-chamriz watershed in Fars province. Model. Earth Syst. Environ. 1, 26. https://doi.org/10.1007/s40808-015-0031-4

Saatsaz, M., 2019. A historical investigation on water resources management in Iran. Environ Dev Sustain. https://doi.org/10.1007/s10668-018-00307-y

Simonneaux, V., Lepage, M., Helson, D., Métral, J., Thomas, S., Duchemin, B., Cherkaoui, M., Kharrou, H., Berjami, B., Chebhouni, A., 2009. Estimation spatialisée de l'évapotranspiration des cultures irriguées par télédétection : application à la gestion de l'irrigation dans la plaine du Haouz (Marrakech, Maroc). Sécheresse 20, 123–130. https://doi.org/10.1684/sec.2009.0177

Soltani, M., Laux, P., Kunstmann, H., Stan, K., Sohrabi, M.M., Molanejad, M., Sabziparvar, A.A., Ranjbar SaadatAbadi, A., Ranjbar, F., Rousta, I., Zawar-Reza, P., Khoshakhlagh, F., Soltanzadeh, I., Babu, C.A., Azizi, G.H., Martin, M.V., 2016. Assessment of climate variations in temperature and precipitation extreme events over Iran. Theor Appl Climatol 126, 775–795. https://doi.org/10.1007/s00704-015-1609-5

Song, Q., Hu, Q., Zhou, Q., Hovis, C., Xiang, M., Tang, H., Wu, W., 2017. In-Season Crop Mapping with GF-1/WFV Data by Combining Object-Based Image Analysis and Random Forest. Remote Sensing 9, 1184. https://doi.org/10.3390/rs9111184

Stancalie, G., Marica, A., Toulios, L., 2010. Using earth observation data and CROPWAT model to estimate the actual crop evapotranspiration. Physics and Chemistry of the Earth, Parts A/B/C, Bio-, Agro, and Urban Climatology 35, 25–30. https://doi.org/10.1016/j.pce.2010.03.013

Su, Z., 2002. The Surface Energy Balance System (SEBS) for estimation of turbulent heat fluxes. Hydrology and Earth System Sciences 6, 85–100. https://doi.org/10.5194/hess-6-85-2002

Tabari, H., Abghari, H., Talaee, P.H., 2012. Temporal trends and spatial characteristics of drought and rainfall in arid and semiarid regions of Iran. Hydrological Processes 26, 3351–3361. https://doi.org/10.1002/hyp.8460

Tasumi, M., 2019. Estimating evapotranspiration using METRIC model and Landsat data for better understandings of regional hydrology in the western Urmia Lake Basin. Agricultural Water Management 226, 105805. https://doi.org/10.1016/j.agwat.2019.105805

Waldhoff, G., Lussem, U., Bareth, G., 2017. Multi-Data Approach for remote sensing-based regional crop rotation mapping: A case study for the Rur catchment, Germany. International Journal of Applied Earth Observation and Geoinformation 61, 55–69. https://doi.org/10.1016/j.jag.2017.04.009

Water Watch, 2019. WaterWatch Remote Sensing Services: Validation [WWW Document]. URL http://www.waterwatch.nl/tools0/sebal/validation.html (accessed 4.8.19).

Waters, R., Allen, R., Tasumi, M., Trezza, R., Bastiaanssen, W., 2002. SEBAL: Surface Energy Balance Algorithms for Land Idaho Implementation Advanced Training and Users Manual. NASA and University of Idaho, Spokane, United States.

Wukelic, G.E., Gibbons, D.E., Martucci, L.M., Foote, H.P., 1989. Radiometric calibration of Landsat Thematic Mapper thermal band. Remote Sensing of Environment 28, 339–347. https://doi.org/10.1016/0034-4257(89)90125-9

Xie, H., Tian, Y.Q., Granillo, J.A., Keller, G.R., 2007. Suitable remote sensing method and data for mapping and measuring active crop fields. International Journal of Remote Sensing 28, 395–411. https://doi.org/10.1080/01431160600702673

Zehtabian, G., Khosravi, H., Ghodsi, M., 2010. High Demand in a Land of Water Scarcity: Iran, in: Water and Sustainability in Arid Regions. Springer, Dordrecht, pp. 75–86. https://doi.org/10.1007/978-90-481-2776-4_5

Zhong, L., 2012. Efficient crop type mapping based on remote sensing in the Central Valley, California. UC Berkeley.

Zwart, S.J., Bastiaanssen, W.G.M., 2007. SEBAL for detecting spatial variation of water productivity and scope for improvement in eight irrigated wheat systems. Agricultural Water Management 89, 287–296. https://doi.org/10.1016/j.agwat.2007.02.002